Composition of the Electrode Determines which Half-Cell's Rate Constant is Higher in a Vanadium Flow Battery

Holger Fink[1], *Jochen Friedl*[2], *Ulrich Stimming*[2,3,*]

[1] *Bavarian Center for Applied Energy Research (ZAE Bayern), Energy Storage, Walther-Meißner-Str. 6, 85748 Garching, Germany*

[2] *School of Chemistry, Bedson Building, Newcastle University, Newcastle upon Tyne, NE1 7RU, United Kingdom*

[3] *TUM CREATE, 1 CREATE Way, #10-02 CREATE Tower, 138602 Singapore*

ABSTRACT: Vanadium Flow Batteries are a promising system for stationary energy storage. One of their shortcomings is a low power-density caused by slow kinetics of the redox reactions. To alleviate this drawback, many studies tried to catalyze the redox reactions. However, up to now, there is no consensus in the literature which of the two half-cell reactions, the V^{2+}/V^{3+}- or the VO^{2+}/VO_2^{+}-reaction, features the slower electron transfer.

The present study is the first showing that reaction rates for the half-cells are of the same order of magnitude with their respective rate constants depending on the composition of the electrode

material.

The surface functional groups hydroxyl, carbonyl and carboxyl on carbon increase the wetted surface area, catalyze the V^{2+}/V^{3+} redox reaction but impede the VO^{2+}/VO_2^{+} redox reaction. This complex situation was unraveled by using a newly developed procedure based on electrochemical impedance spectroscopy. Reaction mechanisms based on these results are discussed.

KEYWORDS: Redox Flow Batteries, Vanadium, Electron Transfer, Catalysis, Kinetics

1. Introduction

Vanadium Flow Batteries (VFB) are a promising system for stationary energy storage and could be useful for grid integration and energy management of renewables or peak shaving[1,2]. For a successful implementation capital cost still have to be reduced, which can be achieved by optimizing all components of the full system[3,4]. One possible point of leverage are the electrodes, for the V^{2+}/V^{3+} as well as for the VO^{2+}/VO_2^{+} half-cell. Optimization of these can be either done by increasing their wetted surface area, or by enhancing their electrochemical activity.

The current state of knowledge regarding the kinetics is compiled in Table 1. It lists studies that compare the electron transfer rate constants k_0 of various carbon electrodes towards the V^{2+}/V^{3+} and VO^{2+}/VO_2^{+} redox reactions. In Table 1 the values for the k_0 spread over three orders of magnitude. Three factors can be identified that influence the activity of an electrode for the two vanadium redox reactions, assuming the current I in an electrochemical experiment is a measure for activity. First, the wetted surface area A^{wet}. Second, the electron transfer rate

constant k_0. Third, the *surface properties of the electrode* which may influence both k_0 and A^{wet}.

$$I \propto k_0(\gamma)\, A^{wet}(\gamma) \quad (1)$$

In this study the amount of functional groups, either hydroxyl or carbonyl and carboxyl combined, and the amount of graphitic carbon will be investigated as potential material properties γ that influence k_0 and A^{wet}.

To give a conclusive answer to which vanadium reaction has the higher k_0, one has to explore the three dimensional parameter space spanned up by k_0, A^{wet} and γ. A closer look at Table 1 reveals that this has not been done before.

Electrode	Method	Results	Ref
GC	CV, SSP	V^{2+}/V^{3+}: k_0=1.0 10^{-6} cm s^{-1} VO^{2+}/VO_2^{+}: k_0=2.2 10^{-6} cm s^{-1}	8
GC	CV, RDE	V^{2+}/V^{3+}: k_0=1.2 10^{-4} cm s^{-1} , "poisoning" of electrode decreases activity VO^{2+}/VO_2^{+}: k_0=7.5 10^{-4} cm s^{-1} , strong dependence on GC preparation stated	9,10
PFC	CV	V^{2+}/V^{3+}: k_0=5.3 10^{-4} cm s^{-1} VO^{2+}/VO_2^{+}: k_0=8.5 10^{-4} cm s^{-1}	11
GF, raw, heat- and acid-treated	CV	V^{2+}/V^{3+}: k_0=1.54 10^{-5} cm s^{-1} VO^{2+}/VO_2^{+}: k_0=1.83 10^{-5} cm s^{-1} both values increase slightly with heat/acid treatment.	12
CP	In-situ polarization	VO^{2+}/VO_2^{+} 44 times faster than V^{2+}/V^{3+}	13
PFC	SSP	VO^{2+}/VO_2^{+} approx. 10 times slower than V^{2+}/V^{3+}	14
CP, GC,	CV	V^{2+}/V^{3+}: k_0=3.5 10^{-5} cm s^{-1} (HOPG) ; 1.1 10^{-3} cm s^{-1} (CP)	15

HOPG		VO^{2+}/VO_2^+: k_0=5.17 10^{-5} cm s^{-1} (HOPG) ; 1.0 10^{-3} cm s^{-1} (CP)	
GC	CV, EIS	Pretreatment of GC at positive potentials actives electrode for V^{2+}/V^{3+}, deactivates for VO^{2+}/VO_2^+	[16]

Table 1: List of studies comparing the rate constants of electrodes towards the V^{2+}/V^{3+} and VO^{2+}/VO_2^+ redox reaction[1].

Yamamura et al. investigated the V^{2+}/V^{3+} and VO^{2+}/VO_2^+ redox reaction on the c-plane of pyrolytic carbon and plastic formed carbon (PFC)[11]. The electron transfer constants were determined by analyzing CV data with the formulas given by Bard and Faulkner for slow redox systems[17]. They also used the $Fe(CN)_6^{3-/4-}$ redox couple to probe the A^{wet} of their electrode. Thus, they determined k_0 and A^{wet} for the two vanadium reactions on their electrodes. But the function $k_0(\gamma)$ may be different for the V^{2+}/V^{3+} and the VO^{2+}/VO_2^+ redox reactions (as we will show later) and therefore their answer, of which reaction is characterized by the higher $k_0(\gamma)$, is correct only on electrodes of exactly the same making as the ones employed in the study.

Agar et al. varied the composition of electrodes and recorded CVs on pristine, acid- and heat-treated graphite felt electrodes[12]. However, they were unable to separate kinetic (k_0) from surface area (A^{wet}) effects on their high-surface area electrode material. In addition, an apparent catalytic effect appears when porous electrode materials are investigated with cyclic voltammetry and was unaccounted for; the porosity reduces the separation between anodic and cathodic peak suggesting enhanced kinetics when indeed only an interplay of enlarged electrochemical surface area and impeded diffusion within the porous electrode is present[6,18].

[1]GC – glassy carbon, PFC – plastic formed carbon, GF – graphite felt, HOPG – highly oriented pyrolytic graphite, CP – carbon paper, CV – cyclic voltammetry, SSP – steady state polarization, RDE – rotating disk electrode, EIS – electrochemical impedance spectroscopy.

Bourke et al. changed the surface composition of a glassy carbon electrode by electrochemical pre-treatment and recorded cyclic voltammograms and electrochemical impedance spectroscopy (EIS) data in electrolytes containing VO^{2+}/VO_2^+ or V^{2+}/V^{3+}[16]. They stated that pretreatment increases the rate constant of V^{2+}/V^{3+} and reduces the rate constant of VO^{2+}/VO_2^+, but it was not clearly resolved whether that altered activity stems from kinetics or surface area effects.

Previously, we presented a method to clearly separate contributions from k_0 and A^{wet} based on the fact that both the charge transfer resistance R_{CT} and the double layer capacitance C_{DL} obtained from EIS are proportional to A^{wet}, which allowed us to determine k_0 unambiguously[6]. This method was employed to investigate the VO^{2+}/VO_2^+ reaction on multi-walled carbon nanotubes (MWCNTs) that were decorated with variable amounts of surface functional groups. This was the first study that showed that for the VO^{2+}/VO_2^+ redox reaction $k_0(\gamma)$ decreases with the amount of surface functional groups γ.

The present study employs the same method to determine the three-dimensional parameter space of electrochemical activity (k_0), surface area (A^{wet}) and surface composition of electrode γ for the vanadium reactions on two commercially available graphite felt electrodes. It will be shown that for the V^{2+}/V^{3+} redox reaction k_0 increases with amount of surface functional groups γ, while it decreases for VO^{2+}/VO_2^+. At the same time, A^{wet} increases with γ for both reactions. This complex behavior for $I \propto k_0(\gamma)\, A^{wet}(\gamma)$ might have led to the contradictory results listed in Table 1. Possible mechanisms that explain the diametric behavior of $k_0(\gamma)$ for the two vanadium reactions will be discussed.

2. Experimental Methods

2.1 Materials and Reagents

All chemicals were analytical grade and used without further purification. Ultra-pure type I water was obtained from a Milli-Q water purification system (Merck Millipore) and was used with sulfuric acid to prepare the supporting electrolyte. The vanadium electrolyte was prepared by electrolysis in a VFB and diluting with *2 M* H_2SO_4 to obtain electrolytes with *50 mM* V^{2+} and *50 mM* V^{3+} (anolyte) or *50 mM* VO^{2+} and *50 mM* VO_2^+ (catholyte).

GFD and GFA graphite felts from SGL Carbon each from one batch were used as electrode material. Both materials are made from fibers that are carbonized and successively graphitized.

2.2 Electrode Preparation and Characterization

For both types of graphite felt electrodes, GFA and GFD, an *untreated*, pristine sample and a heat-treated sample, called *treated*, were prepared. GFD is made from Polyacrylnitrile (PAN) and exhibits a Brunauer-Emmett-Teller (BET) surface area of *0.44* m^2/g [19]. GFA is made from cellulose (Rayon) with a BET surface area of *0.90* m^2/g [19]. Rayon-based felts (GFA) are more easily oxidized to form surface functional groups than PAN-based felts (GFD) because they exhibit a rougher surface microstructure with more edge planes [20]. It is reasonable to assume that the higher surface area of GFA enhances this effect. To achieve comparable degrees of coverage with surface functional groups the heat-treatment was performed for *20 h* in laboratory atmosphere at *400˚C* for GFD and same procedure for *1 h* for GFA. We did not register a significant mass loss (< *1%*) of the electrodes due to heat treatment. Sun reported a mass loss of approximately *1%* when heating a *3 mm* thick graphite felt at *400˚C* for *30 h* in lab atmosphere[21]. Whitehead et al. registered a mass loss *>1%* for a PAN-based graphitic felt only when the material was exposed to temperatures higher than *500˚C* for 2 hours[22].

The preparation of the electrode material is schematically shown in Fig. 1. Cylindrical electrodes are punched out from sheets of graphite felt by hole punches with different diameters (*6, 8, 10* and *12 mm*) and cleaned with N_2 gas. The original thickness of *4.6 mm* for GFD and *6 mm* for GFA was maintained. Prior to electrochemical characterization the electrodes were submersed in electrolyte and filled with it by a vacuum infiltration process. The submersed electrode was exposed to a vacuum in a pressure stable glass container and then pressurized by *Ar*. Repeating this procedure ensured that the felts were entirely wetted with electrolyte. The felts were contacted by centrally piercing them with a cleaned pencil mine (Staedtler, HB, *0.7 mm* diameter, Mars micro carbon). The surface area of the pencil mine which was exposed to the electrolyte was *15* mm^2 for GFD electrodes and *18* mm^2 for GFA electrodes. The approximated BET area exposed to the electrolyte of the smallest felt electrode (GFD, diameter *6 mm*, thickness *4.6 mm*, volume *0.13* cm^3, density *0.11* $g\ cm^{-3}$ [19]) is $6.3 \cdot 10^3\ mm^2$.

The electrode characterization was performed by XPS employing a Thermo Fisher Scientific Theta Probe with a monochromatic X-ray *Al Kα* x-ray source.

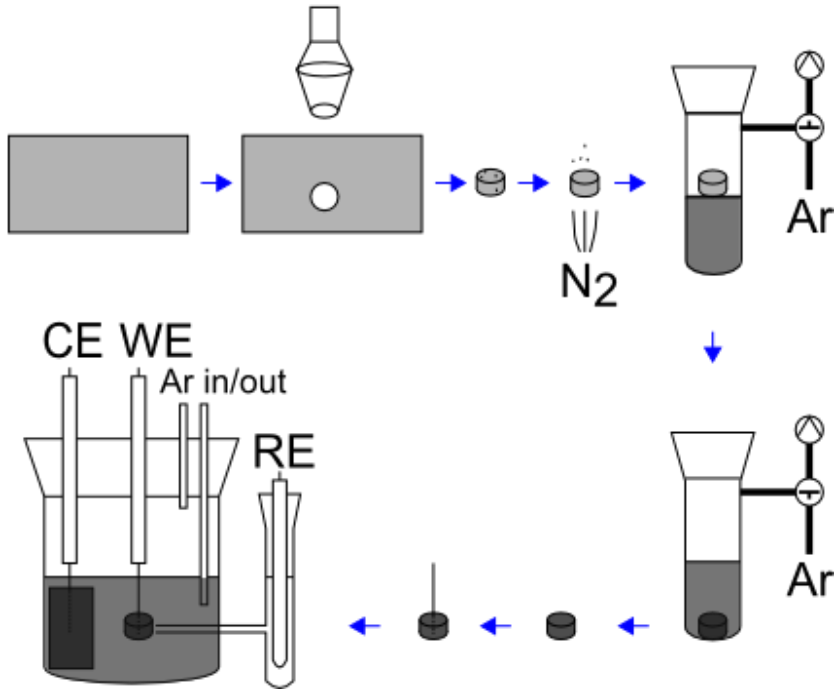

Figure 1: Schematic of the electrode preparation process and the insertion of the electrode in the three-electrode setup. Counter electrode (CE); Working electrode (WE); Reference electrode (RE).

2.3 Electrochemical Setup

A schematic of the electrochemical setup used is shown in Fig. 1. The four different types of sample, GFD untreated, GFD treated, GFA untreated and GFA treated were centrally pierced with a pencil mine and used as working electrodes in a three-electrode setup. This method of contacting the felt was preferred over the alternative contact via a platinum "fish-hook" as it does not introduce a reactive metal into the solution[23]. The pencil mine does not contribute significantly to the signal from the felt electrodes (see Fig. 4) and the recorded ohmic resistances R_{Ohm} do not deviate much for the various measurements. The average values for R_{Ohm} and the standard deviation for all *16* measurements of one kind of graphite felt are: For GFD felts

R_{Ohm}^{GFD} = *(0.97 ± 0.14) Ω* and for GFA felts R_{Ohm}^{GFA} = *(1.13 ± 0.16) Ω.* We assume that a possible non-uniform current distribution within the felt does not introduce a significant systematic error because the amplitude used in the EIS measurements is only *10 mV* and therefore the current density within the electrode is small.

In a custom-built glass-cell a gold sheet (in catholyte) and a piece of graphite felt (*10 cm²*, in anolyte) served as counter electrodes. A Mercury/Mercourus Sulfate electrode in *2 M* H_2SO_4 (MSE, *0.67 V* vs. Normal Hydrogen Electrode (NHE)[24]) was used as reference electrode. All potentials reported are recalculated to NHE. Before each measurement the electrolyte was purged for at least *15 min* with argon to remove dissolved oxygen from the solution.

A Bio-Logic SP-240 potentiostat was used for potential control and data acquisition.

2.4. Evaluation of Electron Transfer Kinetics

A novel method to extract kinetic information for rough and also porous structures was described in reference[6]. It was developed because potential scanning methods are not suitable for porous, high surface area electrode[6,18,25], and values for the surface area based on BET might be largely different from the wetted surface area A^{wet} [26]. Equations for charge transfer resistance R_{CT},

$$R_{CT} = \frac{R\,T}{n\,F\,j_0 A^{wet}} \tag{2}$$

and double layer capacitance C_{DL},

$$C_{DL} = \varepsilon_r \varepsilon_0 \frac{A^{wet}}{t_{DL}} \tag{3}$$

contain besides the exchange current density j_0, the gas constant R, the absolute temperature T, number of transferred electrons n, Faraday constant F, relative dielectric permeability ε_r,

permittivity of free space ε_0 and the thickness of the double layer t_{DL} the wetted surface area A^{wet}. Simple substitution leads to:

$$R_{CT}^{-1} = \frac{n\,F\,t_{DL}}{R\,T\,\varepsilon_r\varepsilon_0}\, j_0\, C_{DL} \qquad (4)$$

This indicates that R_{CT} decreases inversely with C_{DL} and that the slope of Eq. 4 yields the kinetic information j_0 (which is directly proportional to k_0) unambiguously. This method was applied for elucidating the kinetic parameters of the redox system and the electrodes used in this study.

3. Results

3.1 Characterization of Electrode Material

The felt samples were investigated by XPS to assess the influence of the heat treatment on the surface composition. The *C1s* spectra were fitted with distributions for the binding energies for graphitic carbon (*C-C, 284.5 eV*), hydroxyl groups (*C-OH, 285.0 eV*) and carbonyl and carboxyl (*C=O* and *O-C=O, 286.0 eV*). The spectra with fitted curves for all four samples are shown in Figure S1. The relative surface concentration of various species can be estimated from the peak sizes[27]. The atomic composition of the surface for the four samples is shown in Figure 2. Heat treatment increases the amount of hydroxyl, carbonyl and carboxyl functional groups on the surface of GFD and GFA graphite felts. This increase in functional groups with heat treatment is well documented for graphite felts, both PAN- and Rayon-based[20,21,28,29]. It has also been reported that Rayon-based fibers form oxygen containing surface groups upon oxidative treatment faster than PAN-based fibers[20], therefore we chose the GFA heat-treatment to be shorter. Nevertheless, on GFA more oxygen containing functional groups are generated than on

GFD. For activated carbon it was shown that thermal treatment at *425˚C* increases the amount of carbonyl and hydroxyl groups, which fits well with our observation[30].

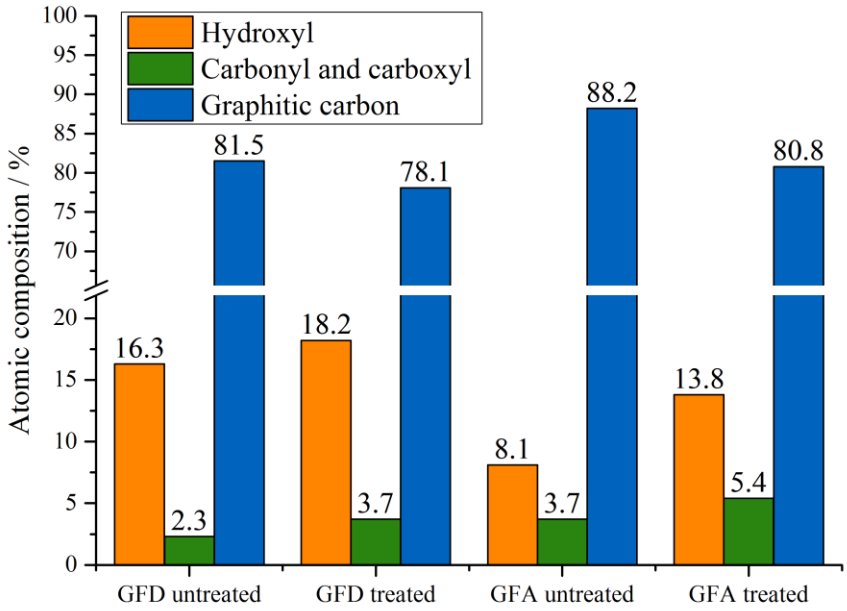

Figure 2: Composition of graphite felt samples as determined from *C1s* XPS spectra.

3.2 Investigation of the Redox Reaction in the Catholyte

For the kinetic evaluation of the electrodes in the catholyte graphite felts with varying sizes were immersed in electrolyte containing *50 mM* VO^{2+} and *50 mM* VO_2^+ in *2 M* H_2SO_4, henceforth called *catholyte*. EIS was performed at the open circuit potential (OCP) of the cell $U_{OCP} = 0.97\ V$ vs. NHE which corresponds well with the standard potential $U_0 = 1.00\ V$ vs. NHE[31]. Nyquist plots for sample GFD untreated are shown in Fig. 3a. From these it is obvious that with increasing electrode diameter (volume) R_{CT} decreases. Fig. 3b gives one exemplary Bode representation for a GFD untreated electrode with a diameter of *6 mm* and volume *0.13* cm^3.

To extract quantitative values all spectra were fitted with the equivalent circuit shown in Fig. 3a.

Except for frequencies larger than 10^5 *Hz* the fit does not deviate from the experimental data. The constant phase element (CPE) was transformed to C_{DL} using the formula given by Hirschorn et al. for a surface time-constant distribution [32]. The CPE parameter α was always $0.94 < \alpha < 1$.

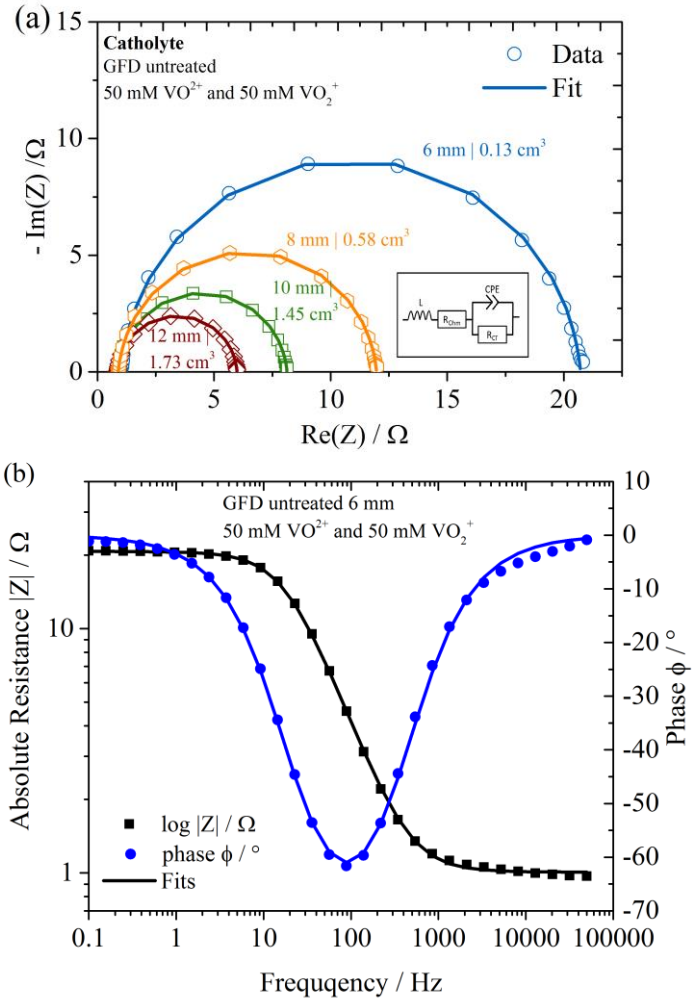

Figure 3: Electrochemical impedance spectroscopy results for GFD untreated in the catholyte. The fits to the data points are shown as solid lines (a) Nyquist plots of four electrodes with diameters from *6* to *12 mm*. The equivalent circuit used for the fitting is shown in the inset. (b) Exemplary Bode plot of the *6 mm* electrode.

Extracted values for C_{DL} and R_{CT}^{-1} for all four electrode materials are shown in Fig. 4. Also R_{CT}^{-1} and C_{DL} determined for the pencil mine sample holder are shown as black data point adjacent to the origin.

As Eq. 4 predicts, all data points can be fitted linearly, R_{CT} decreases with increasing C_{DL}. This slope is a measure for j_0 and can be used to compare electrode materials and redox couples[6]. It varies for the electrode materials and the untreated samples have a larger slope than the heat-treated samples.

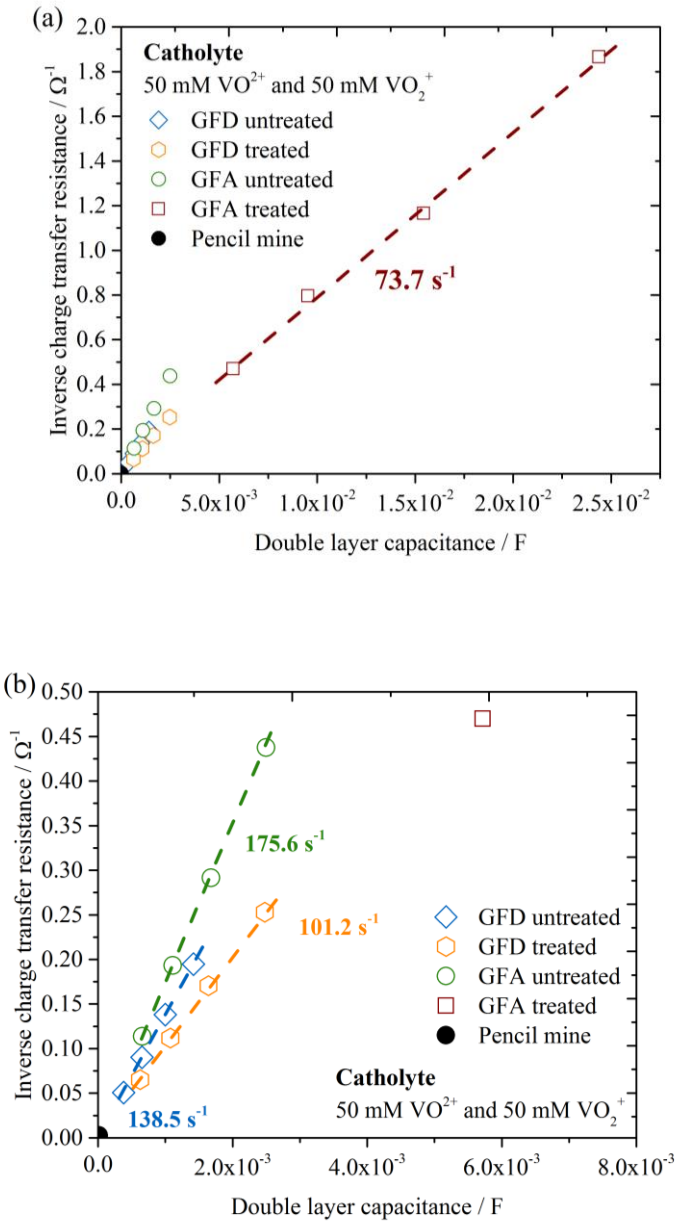

Figure 4: (a) Inverse charge transfer resistance (R_{CT}^{-1}) plotted over the double layer capacitance (C_{DL}) in the catholyte for the four electrode materials under investigation. (b) Details for lower capacitances.

3.3 Investigation of the Redox Reaction in the Anolyte

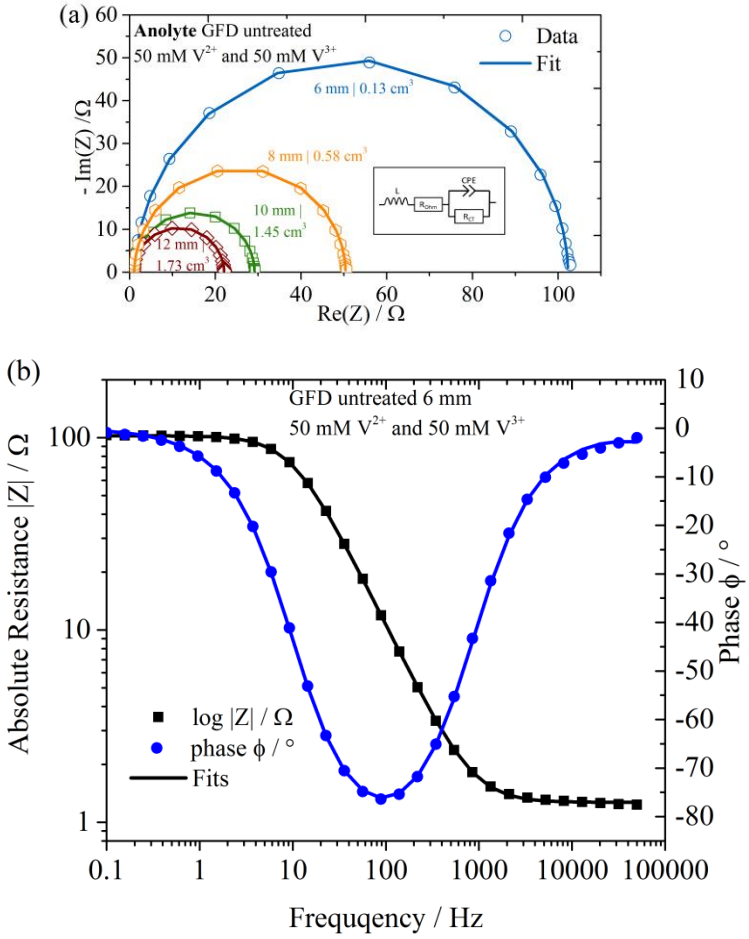

Figure 5: Electrochemical impedance spectroscopy results for GFD untreated in the anolyte. The fits to the data points are shown as solid lines. (a) Nyquist plots of four electrodes with diameters from *6* to *12 mm*. The equivalent circuit used for the fitting is shown in the inset. (b) Exemplary Bode plot of the *6 mm* electrode.

The same process as described in section 3.2 was performed for an electrolyte containing *50 mM* V^{2+} and *50 mM* V^{3+} in *2 M* H_2SO_4, henceforth called *anolyte*. The EIS was conducted at U_{OCP} = *-0.22 V* vs. NHE which corresponds well with the standard potential U_0 = *-0.26 V* vs. NHE given in the literature[31]. Exemplary EIS data with fitted curves and equivalent circuit are shown in Fig. 4 for untreated GFD felt electrodes. As before, larger electrodes are characterized

by smaller semicircles. Values for C_{DL} and R_{CT}^{-1} are calculated and shown in Fig. 6 for all electrode materials. The CPE parameter α was always $0.89 < \alpha < 1$.

This time, the sequence observed is different than in the catholyte. The treated samples exhibit higher slopes than the untreated samples which indicate a higher j_0 for the V^{2+}/V^{3+} reaction on treated samples.

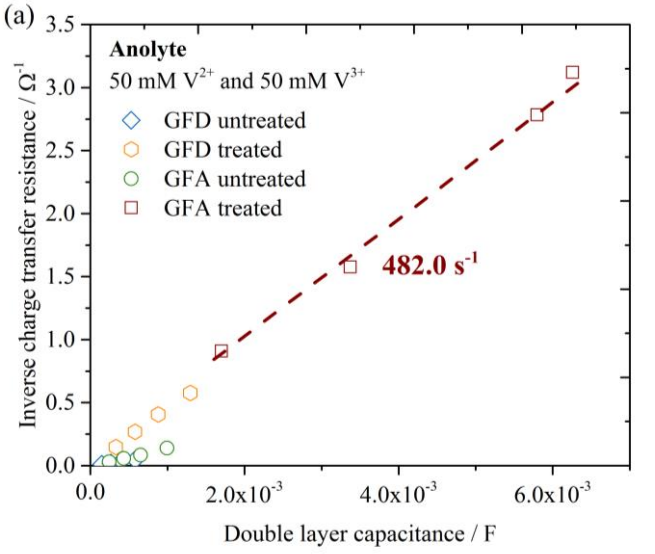

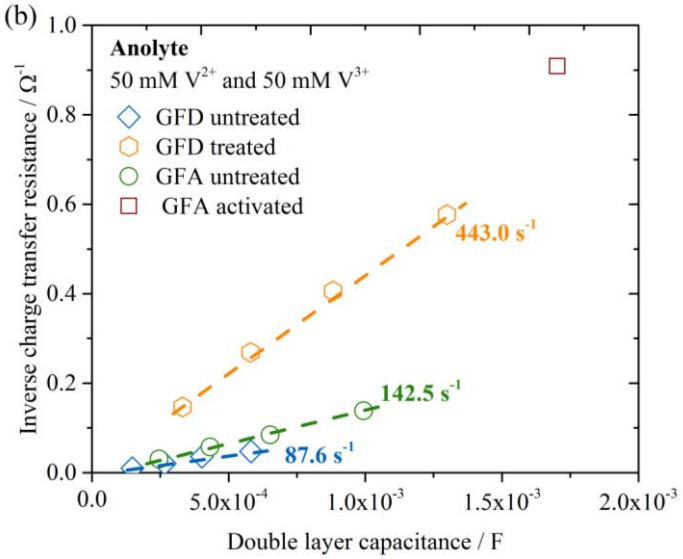

Figure 6: (a) Inverse charge transfer resistance (R_{CT}^{-1}) plotted over the double layer capacitance (C_{DL}) in the anolyte for the four electrode materials under investigation. (b) Detail for lower capacitances.

3.4 Double Layer Capacitance versus Potential

As the EIS data for anolyte and catholyte were recorded at different potentials, the change of C_{DL} with potential has to be taken into account, in order to compare the slopes and therefore the rate constants of the V^{2+}/V^{3+} and the VO^{2+}/VO_2^{+} reaction correctly.

For this purpose EIS measurements were performed for all four graphite felts under investigation in *2 M* H_2SO_4 from *-0.33 V* to *1.17 V* vs. NHE. The obtained data points were fitted to an equivalent circuit comprising a resistance and a CPE in series. The CPE was converted to C_{DL} using the formula for a surface distribution of time-constants and infinite charge transfer resistance[32]. The CPE parameter α was always $0.87 < \alpha < 1$. Exemplary curves for GFD untreated with a diameter of *10 mm* are shown in Fig. S2.

Combining these EIS measurements gives curves as shown in Fig. 7. For GFD untreated the measurement was performed three times with electrodes of the same size to confirm the reproducibility of the curves. The curve shown is the average of those three measurements and the error bars are the standard deviation. The double layer capacitance is higher at the standard potential of the VO^{2+}/VO_2^{+} reaction ($C_{DL}^{VO^{2+}/VO_2^{+}}$) than at that of the V^{2+}/V^{3+} reaction ($C_{DL}^{V^{2+}/V^{3+}}$). This is true for all the investigated electrodes. To adjust for this we introduce a correction factor β:

$$\beta = \frac{C_{DL}^{VO^{2+}/VO_2^{+}}}{C_{DL}^{V^{2+}/V^{3+}}} \qquad (5)$$

The correction factors for all electrode materials are given in Table 2. When comparing rate constants for the two redox reactions the potential dependency of C_{DL} has to be taken into account. Slopes multiplied with unity (for V^{2+}/V^{3+}) or the correction factor β (for VO^{2+}/VO_2^{+}) are called normalized rate constants.

The shape of the curves in Figure 7 can be explained by a superposition of two effects:

- According to the Guy-Chapman theory the C_{DL} over potential curve has roughly the shape of a parabola with the minimum at the potential of zero charge of the electrode[33];
- Surface functional groups undergo redox reactions at two potentials in the potential window shown in Figure 7, at $U^1 = 0.27$ *V vs. NHE* and at $U^2 = 0.67$ *V vs. NHE*[34]. The first peak at U^1 was assigned to carbonyl and hydroxyl groups, the peak at U^2 to quinone/hydroquinone groups[34]. Thermal treatment increases the charges transferred during these reactions.

A peak in the C_{DL} around U^2 is visible in Fig. 7 for both samples and for GFD treated another peak at U^1 becomes apparent. In Table 2 β is always larger for untreated that for treated samples. This might be due to the contribution of the carbonyl and hydroxyl groups at U^1 which is close to the standard potential of the V^{2+}/V^{3+} reactions and therefore contributes more to $C_{DL}^{V^{2+}/V^{3+}}$ than to $C_{DL}^{VO^{2+}/VO_2^{+}}$, thereby diminishing the discrepancy between the two capacitances.

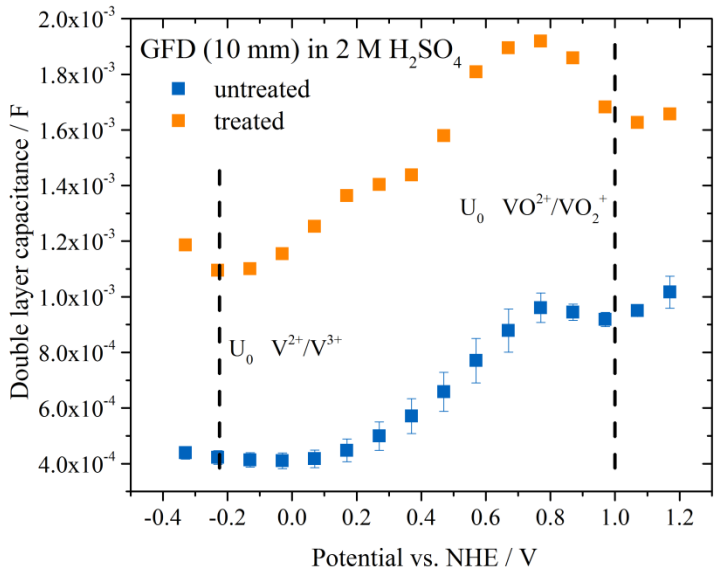

Figure 7: Double layer capacitance C_{DL} vs. the potential in *2 M H_2SO_4* without redox-couple for the GFD samples (10 mm samples). The data points were obtained from a fit of impedance spectra to an equivalent circuit consisting of serial connection of a resistance and a constant phase element (shown in the SI).

Electrode	GFD untreated	GFD treated	GFA untreated	GFA treated
Correction factor β	*2.27*	*1.48*	*2.49*	*1.89*

Table 2: List of correction factors for the difference in double layer capacitance determined from plots as shown in Fig. 7 according to Eq. 5.

4. Discussion and Conclusions

The XPS results shown in Fig. 2 allow generalizing our findings. The wetted surface area of the electrode $A^{wet}(\gamma)$ and the electrochemical activity $k_0(\gamma)$ can be plotted versus material properties γ.

The specific gravimetric double layer capacitance c_{DL} (F/g) of the four samples in anolyte and catholyte was obtained by plotting the corrected C_{DL} over the measured mass of the electrodes and determining the respective slopes, as shown in Figure S3. In this case, $C_{DL}^{V^{2+}/V^{3+}}$ was multiplied by unity and $C_{DL}^{VO^{2+}/VO_2^+}$ was divided by β. Fig. 8a shows the c_{DL} (obtained from Fig. S3) for all samples versus the amount of carbonyl and carboxyl on the surface of the electrode. For both electrode materials an increase in the functional groups increases the $c_{DL.}$ As C_{DL} is directly proportional to A^{wet}, we assume that an increase in functional groups increases A^{wet}. This effect is more pronounced for GFA than it is for GFD and independent of which vanadium redox reaction takes place [7]. If the amount of hydroxyl groups is selected as abscissa the behavior is qualitatively the same. One interpretation is that an increase in the functional groups increases A^{wet} by increasing the hydrophilicity of the sample, as described for carbon nanotubes[7]. Another interpretation is that the heat treatment increases the actual surface area of the electrode, as it might create pores or defects and thereby increase the A^{wet}. Most likely both phenomena contribute to the increase in A^{wet}. Their exact attribution is beyond the scope of this study.

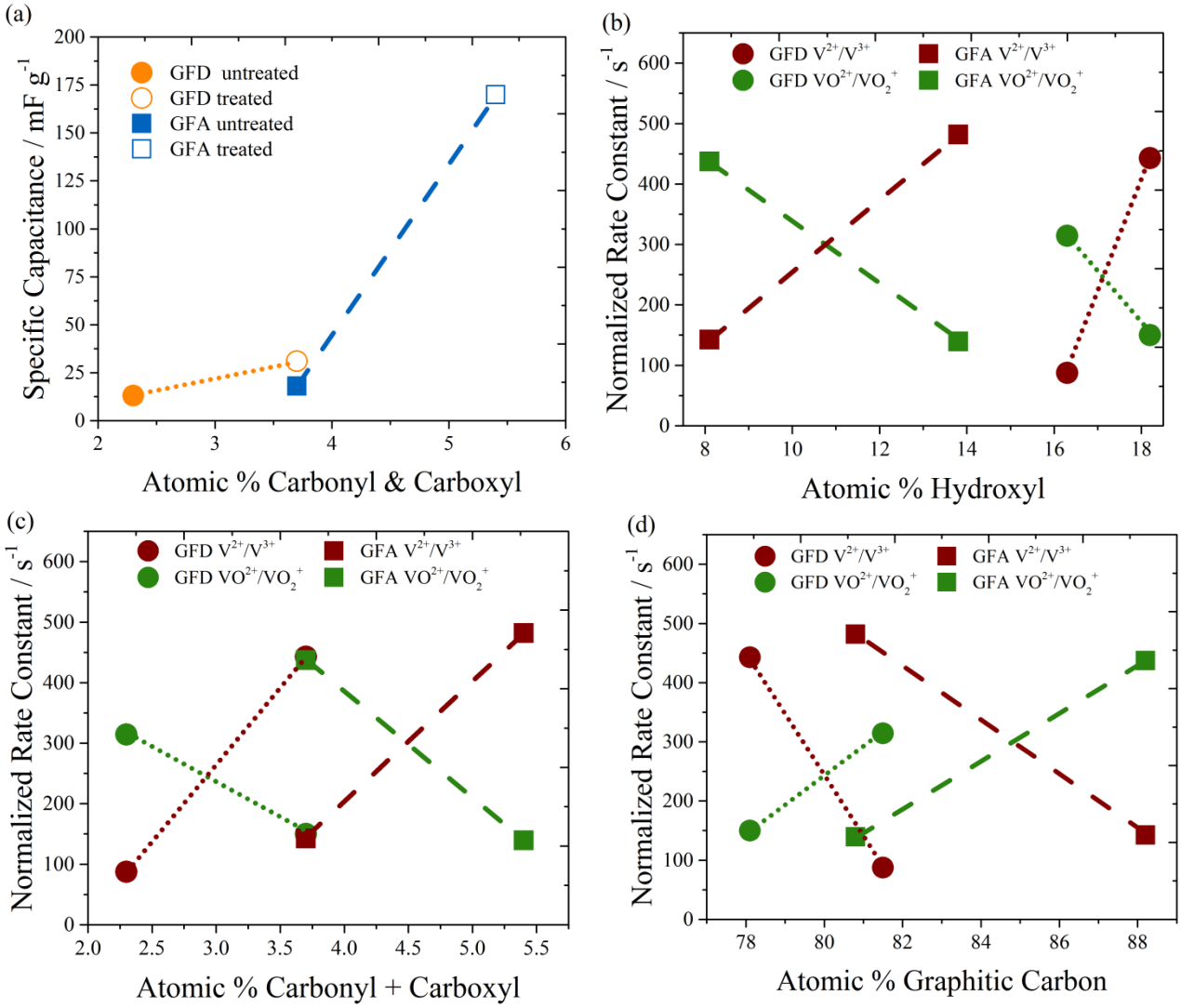

Figure 8: (a) Specific gravimetric capacitance over carbonyl and carboxyl as determined from XPS. Normalized rate constants for the V^{2+}/V^{3+} (red) and the VO^{2+}/VO_2^{+} (green) redox reactions for the two electrode materials GFD (circle) and GFA (square) plotted over atomic % of carbon groups as determined by XPS: (b) hydroxyl, (c) carbonyl and carboxyl and (d) graphitic carbon.

For the electrochemical rate constants $k_0(\gamma)$ the situation is more complicated. In general it is established that oxidative treatment increases defect density (edge plane sites, sp^3 hybridization)

which typically leads to an increased amount of surface oxygen, therefore more reaction sites and hence accelerated electrochemical rates[35]. From XPS measurements we obtained material properties that are likely to influence electrochemical properties. They are atomic % of the XPS sampling space of hydroxyl (Fig. 8b), carbonyl and carboxyl (Fig. 8c) and graphitic carbon (Fig. 8d).

The results from Fig. 8b-d can be summarized as follows:

- The normalized rate constants for the V^{2+}/V^{3+} redox reaction increase with increasing amount of hydroxyl (Fig. 8b) or carbonyl and carboxyl (Fig. 8c) and decrease with increasing amount of graphitic carbon (Fig. 8d);
- The normalized rate constants for the VO^{2+}/VO_2^{+} redox reaction decrease with increasing amount of hydroxyl (Fig. 8b) or carbonyl and carboxyl (Fig. 8c) and increase with increasing amount of graphitic carbon (Fig. 8d);
- The trends for the two redox reactions are always diametrical, increasing normalized rate constants for one redox reaction is accompanied by a decrease in normalized rate constants for the other;
- The trends described above hold true independently of the type of felt electrode, GFA or GFD. In Fig. 8c the slopes for the changes are similar for GFA and GFD.

Figure 8b and 8c indicate that the important material property γ that determines $k_0(\gamma)$ is the amount of functional groups hydroxyl, carbonyl and carboxyl. Figure 8d points towards the importance of crystallinity as γ. As an increase in sp^3 hybridized carbon comes at the cost of sp^2 hybridized carbon it is very difficult to separate the two properties experimentally. Looking at the literature we can propose reaction mechanisms that are consistent with the results shown in Fig.8b-c.

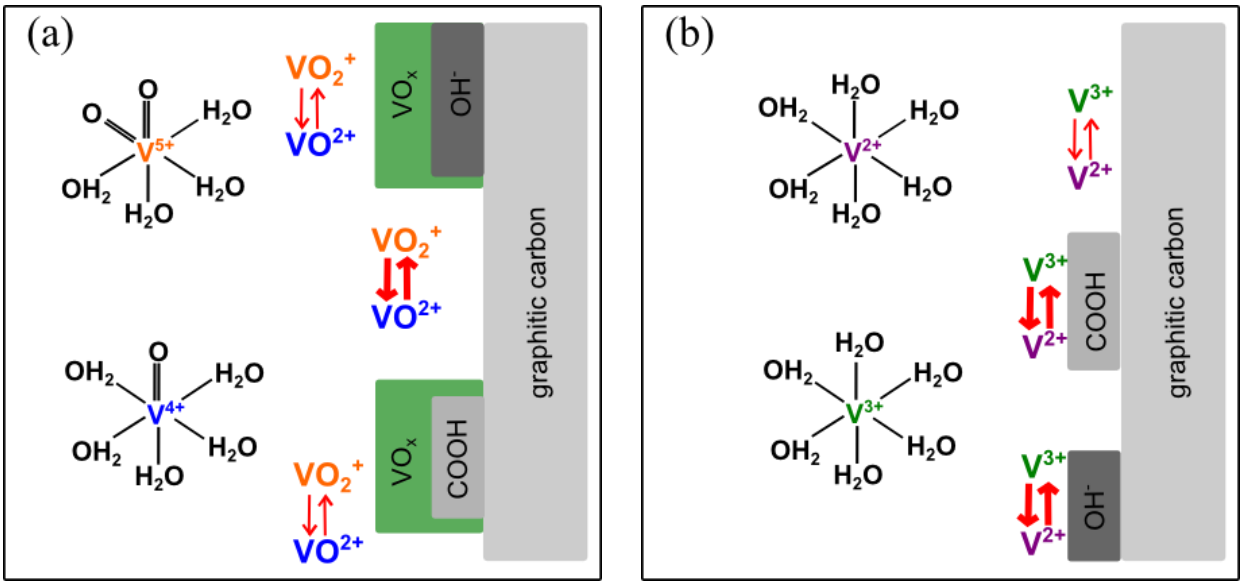

Figure 9: Possible reaction mechanisms for the VO^{2+}/VO_2^+ (a) and the V^{2+}/V^{3+} (b) redox reaction that are consistent with the results shown in Fig. 8. The line width of arrows indicates reaction rate. (a) On functional surface groups vanadium species from the solution chemisorb and form a passivating film of vanadium oxides. (b) Surface functional groups catalyze the V^{2+}/V^{3+} redox reaction either by an electrostatic effect or through a bridge-activated electron transfer.

The mechanism schematically shown in Fig. 9a combines our findings with X-Ray Absorption Fine Structure (XAFS) results by Maruyama et al.[36]: XAFS measurements indicate the presence of adsorbed vanadium oxides on a carbon electrode after immersion in an electrolyte containing *50 mM* VO^{2+} and *50 mM* VO_2^+ [36]. As the interaction of the solvated ions and the carbon surface is expected to be weak, the vanadium ions are assumed to be chemisorbed on oxygen-functional groups on the carbon surface[37]. Our results and previous studies of the kinetics show that oxygen-functional groups impede the VO^{2+}/VO_2^+ redox reaction[6,16,38]. Therefore we hypothesize that vanadium oxides chemisorb on the felt electrodes at these oxygen surface groups and in the process passivate parts of the electrode for the redox reaction. Such passivation layers were

previously described in the literature, for example an oxide layer on iron electrodes that impedes the $[Fe(CN)_6]^{4-}/[Fe(CN)_6]^{3-}$ redox reaction was investigated[39]. Gattrell et al. also proposed a formation of vanadium oxides at the electrode from the observation of a low apparent symmetry factor during rotating disk electrode studies[40].

An alternative explanation for the impeding influence of functional groups on the rate of the VO^{2+}/VO_2^{+} was given by Melke et al.[41]. Employing Near Edge X-ray absorption spectroscopy (NEXAFS) and cyclic voltammetry they correlated a higher ratio of sp^2- to sp^3-carbon with lower potential position of the oxidation peak in the CV and therefore a higher activity. As a higher content of oxygen functional groups correlates with an increase in sp^3 carbon and a decrease in sp^2 carbon content, the observation from Melke et al. matches the findings presented in Figure 8d. Instead of the reaction mechanism presented in Fig. 9a the study concludes that a low amount of sp^2-carbon (57% for the sample with the lowest activity) leads to a low conductivity within the electrode and ”electron transport in the solid limits the charge transfer process”[41]. But a low conductivity of the electrode should manifest itself in a high ohmic drop R_{Ohm} in EIS measurements. We find the R_{CT} to be always larger than R_{Ohm}, and R_{Ohm} relatively constant regardless of the sample.

Hung and Nagy stated that the rate of electron transfer in the ferrous/ferric system is significantly slowed down when chloride ions are removed from the electrolyte[42]. The same effect was found by Weber et al.[43]. As Fe^{2+}/Fe^{3+} and V^{2+}/V^{3+} are in the same classification of redox system, that is *surface sensitive* and *oxide sensitive*[5], we hypothesize that the presence of surface oxides has a similar effect as the chloride ions and catalyzes the redox reactions either via:

- An electrostatic effect as the surface oxide perturbs the interfacial potential distribution of the transition complex, or;
- A bridge-activated charge transfer mechanism during which the functional group is incorporated into the first coordination shell of the reactant. The charge transfer then proceeds via the formed bridge and can be classified as inner-sphere mechanism.

This mechanism is schematically shown in Fig. 9b.

In this study we investigated the redox reactions important for the VFB, V^{2+}/V^{3+} and VO^{2+}/VO_2^{+}. We studied how the electron transfer constant k_0, wetted surface area A^{wet} and amount of surface functional groups γ influence the current on graphite felt electrodes. By clearly distinguishing the effects brought about by $k_0(\gamma)$ and $A^{wet}(\gamma)$ we showed that the question which reaction is faster is tied to the question which electrode material is used and how it was treated prior to the measurement. Reaction mechanisms were proposed that are consistent with the experimentally found dependence of reaction rate on material properties of the electrodes and with literature data.

Supporting Information

The supporting information gives details on the C1s scan XPS spectra of the four graphite felt samples, EIS spectra of an electrode in *2 M* H_2SO_4 without any redox species and a plot of the double layer capacitance over mass of the electrodes.

This material is available free of charge via the Internet at http://pubs.acs.org/.

Author Information

Corresponding author: Ulrich Stimming: ulrich.stimming@newcastle.ac.uk

Author contributions: The manuscript was written through contributions of all authors. All authors have given approval to the final version of the manuscript.

Acknowledgments

This work was financially supported by Campus for Research Excellence and Technological Enterprise (CREATE) program, Singapore, by the Bavarian Ministry of Economic Affairs and Media, Energy and Technology at the ZAE Bayern (project ZAE storage technologies), Germany and Newcastle University, United Kingdom. We also would like to thank SGL Carbon for the kind provision of graphite felt samples.

References

(1) Parasuraman, A.; Lim, T. M.; Menictas, C.; Skyllas-Kazacos, M. Review of Material Research and Development for Vanadium Redox Flow Battery Applications. *Electrochim. Acta* **2013**, *101* (2010), 27–40.

(2) Weber, A. Z.; Mench, M. M.; Meyers, J. P.; Ross, P. N.; Gostick, J. T.; Liu, Q. Redox Flow Batteries: A Review. *J. Appl. Electrochem.* **2011**, *41* (10), 1137–1164.

(3) Darling, R.; Gallagher, K. G.; Kowalski, J. a; Ha, S.; Brushett, F. R. Pathways to Low-Cost Electrochemical Energy Storage: A Comparison of Aqueous and Nonaqueous Flow Batteries. *Energy Environ. Sci.* **2014**, 3459–3477.

(4) Zhang, M.; Moore, M.; Watson, J. S.; Zawodzinski, T. a.; Counce, R. M. Capital Cost Sensitivity Analysis of an All-Vanadium Redox-Flow Battery. *J. Electrochem. Soc.* **2012**, *159* (8), A1183–A1188.

(5) McCreery, R. L. Advanced Carbon Electrode Materials for Molecular Electrochemistry. *Chem. Rev.* **2008**, *108* (7), 2646–2687.

(6) Friedl, J.; Bauer, C. M.; Rinaldi, A.; Stimming, U. Electron Transfer Kinetics of the – Reaction on Multi-Walled Carbon Nanotubes. *Carbon N. Y.* **2013**, *63*, 228–239.

(7) LI, L.; LI, F. The Effect of Carbonyl, Carboxyl and Hydroxyl Groups on the Capacitance of Carbon Nanotubes. *New Carbon Mater.* **2011**, *26* (3), 224–228.

(8) Oriji, G.; Katayama, Y.; Miura, T. Investigations on V(IV)/V(V) and V(II)/V(III) Redox Reactions by Various Electrochemical Methods. *J. Power Sources* **2005**, *139* (1-2), 321–324.

(9) Sum, E.; Skyllas-Kazacos, M. A Study of the V (II)/V (III) Redox Couple for Redox Flow Cell Applications. *J. Power Sources* **1985**, *15*, 179–190.

(10) Sum, E.; Rychcik, M.; Skyllas-Kazacos, M. Investigation of the V (V)/V (IV) System for Use in the Positive Half-Cell of a Redox Battery. *J. Power Sources* **1985**, *16*, 85–95.

(11) Yamamura, T.; Watanabe, N.; Yano, T.; Shiokawa, Y. Electron-Transfer Kinetics of Np3+/Np4+, NpO2+/NpO22+, V2+/V3+, and VO2+/VO2+ at Carbon Electrodes. *J. Electrochem. Soc.* **2005**, *152* (4), A830.

(12) Agar, E.; Dennison, C. R.; Knehr, K. W.; Kumbur, E. C. Identification of Performance Limiting Electrode Using Asymmetric Cell Configuration in Vanadium Redox Flow Batteries. *J. Power Sources* **2013**, *225*, 89–94.

(13) Aaron, D.; Sun, C.-N.; Bright, M.; Papandrew, a. B.; Mench, M. M.; Zawodzinski, T. a. In Situ Kinetics Studies in All-Vanadium Redox Flow Batteries. *ECS Electrochem. Lett.* **2013**, *2* (3), A29–A31.

(14) Fabjan, C.; Garche, J.; Harrer, B.; Jörissen, L. The Vanadium Redox-Battery: An Efficient Storage Unit for Photovoltaic Systems. *Electrochim. Acta* **2001**, *47*, 825–831.

(15) Wu, X. W.; Yamamura, T.; Ohta, S.; Zhang, Q. X.; Lv, F. C.; Liu, C. M.; Shirasaki, K.; Satoh, I.; Shikama, T.; Lu, D.; et al. Acceleration of the Redox Kinetics of VO2+/VO2 + and V3+/V2+ Couples on Carbon Paper. *J. Appl. Electrochem.* **2011**, *41* (10), 1183–1190.

(16) Bourke, A.; Quill, N.; Lynch, R. P.; Buckley, D. N. Effect of Pretreatment on the Rate of the VO2+/VO2+ and V2+/V3+ Reactions at a Carbon Electrode. *ECS Trans.* **2014**, *61* (37), 15–26.

(17) Bard, A.; Faulkner, L. *Electrochemical Methods: Fundamentals and Applications*, Second.; Harris, D., Swain, E., Robey, C., Aiello, E., Eds.; John Wiley and Sons: New York, 2001.

(18) Punckt, C.; Pope, M. A.; Aksay, I. A. On the Electrochemical Response of Porous Functionalized Graphene Electrodes. *J. Phys. Chem. C* **2013**, *117* (31), 16076–16086.

(19) Schweiss, R.; Oelsner, T.; Dörfler, F.; Davydov, A.; Wöhner, S. Recent Insights into Carbon Felt Electrodes for Redox Flow Batteries. In *International Flow Battery Forum 2011*; 2011; pp 44–45.

(20) Zhong, S.; Padeste, C.; Kazacos, M.; Skyllas-Kazacos, M. Comparison of the Physical, Chemical and Electrochemical Properties of Rayon- and Polyacrylonitrile-Based Graphite Felt Electrodes. *J. Power Sources* **1993**, *45* (1), 29–41.

(21) Sun, B. Modification of Graphite Electrode Materials. *Electrochim. Acta* **1992**, *37* (1), 1253–1260.

(22) Rabbow, T. J.; Trampert, M.; Pokorny, P.; Binder, P.; Whitehead, A. H. Variability within a Single Type of Polyacrylonitrile-Based Graphite Felt after Thermal Treatment. Part I:

Physical Properties. *Electrochim. Acta* **2015**, *173*, 17–23.

(23) Smith, R. E. G.; Davies, T. J.; Baynes, N. de B.; Nichols, R. J. The Electrochemical Characterisation of Graphite Felts. *J. Electroanal. Chem.* **2015**, *747*, 29–38.

(24) Uhlemann, M.; Krause, A.; Chopart, J. P.; Gebert, A. Electrochemical Deposition of Co under the Influence of High Magnetic Fields. *J. Electrochem. Soc.* **2005**, *152* (12), C817.

(25) Punckt, C.; Pope, M.; Aksay, I. High Selectivity of Porous Graphene Electrodes Solely due to Transport and Pore Depletion Effects. *J. Phys. Chem. C* **2014**.

(26) Lehman, J. H.; Terrones, M.; Mansfield, E.; Hurst, K. E.; Meunier, V. Evaluating the Characteristics of Multiwall Carbon Nanotubes. *Carbon N. Y.* **2011**, *49* (8), 2581–2602.

(27) Boehm, H. P. Surface Oxides on Carbon and Their Analysis: A Critical Assessment. *Carbon N. Y.* **2002**, *40* (2), 145–149.

(28) Kim, K. J.; Kim, Y. J.; Kim, J. H.; Park, M. S. The Effects of Surface Modification on Carbon Felt Electrodes for Use in Vanadium Redox Flow Batteries. *Mater. Chem. Phys.* **2011**, *131* (1-2), 547–553.

(29) Chakrabarti, M. H.; Brandon, N. P.; Hajimolana, S. A.; Tariq, F.; Yufit, V.; Hashim, M. A.; Hussain, M. A.; Low, C. T. J.; Aravind, P. V. Application of Carbon Materials in Redox Flow Batteries. *J. Power Sources* **2014**, *253*, 150–166.

(30) Figueiredo, J.; Pereira, M.; Freitas, M.; Orfao, J. Modification of the Surface Chemistry of Activated Carbons. *Carbon N. Y.* **1999**, *37*, 1379–1389.

(31) International Union of pure and applied Chemistry. *Standard Potentials in Aqueous Solution.*; Bard, A. J., Parsons, R., Jordan, J., Eds.; CRC Press: New York, 1985; Vol. 17.

(32) Hirschorn, B.; Orazem, M. E.; Tribollet, B.; Vivier, V.; Frateur, I.; Musiani, M. Determination of Effective Capacitance and Film Thickness from Constant-Phase-Element Parameters. *Electrochim. Acta* **2010**, *55* (21), 6218–6227.

(33) Delahay, P. Double Layer Studies. *J. Electrochem. Soc.* **1966**, *113*, 967.

(34) Rabbow, T. J.; Trampert, M.; Pokorny, P.; Binder, P.; Whitehead, A. H. Variability within a Single Type of Polyacrylonitrile-Based Graphite Felt after Thermal Treatment. Part II: Chemical Properties. *Electrochim. Acta* **2015**, *173*, 24–30.

(35) Frysz, C. A.; Shui, X.; Chung, D. D. L. Effect of Chemisorbed Oxygen on the Electrochemical Behavior of Graphite Fibers. *Carbon N. Y.* **1994**, *32* (8), 1499–1505.

(36) Maruyama, J.; Shinagawa, T.; Hayashida, A.; Matsuo, Y.; Nishihara, H.; Kyotani, T. Vanadium Ion Redox Reactions in Three-Dimensional Network of Reduced Graphite Oxide. *ChemElectroChem* **2015**, n/a – n/a.

(37) Kustin, K.; Liu, S.-; Nicolini, C.; Toppen, D. Interaction of Catechol and Catechol Derivatives with Dioxovanadium:(V). I. Kinetics of Complex Formation in Acidic Media. *J. Am. Chem. Soc.* **1974**, *96* (24), 7410–7415.

(38) Bourke, A.; Lynch, R. P.; Buckley, D. N. Effect of Electrode Pretreatment on the Cyclic Voltammetry of VO2+/VO2+ at a Glassy Carbon Electrode. *ECS Trans.* **2013**, *53* (30),

59–67.

(39) Meisterjahn, P.; Schultze, J. W.; Siemensmeyer, B.; Stimming, U.; Dean, M. H. Electron Transfer Reactions on Passive Iron Electrodes. *Chem. Phys.* **1990**, *141* (1), 131–141.

(40) Gattrell, M.; Qian, J.; Stewart, C.; Graham, P.; MacDougall, B. The Electrochemical Reduction of VO2+ in Acidic Solution at High Overpotentials. *Electrochim. Acta* **2005**, *51* (3), 395–407.

(41) Melke, J.; Jakes, P.; Langner, J.; Riekehr, L.; Kunz, U.; Zhao-Karger, Z.; Nefedov, A.; Sezen, H.; Wöll, C.; Ehrenberg, H.; et al. Carbon Materials for the Positive Electrode in All-Vanadium Redox Flow Batteries. *Carbon N. Y.* **2014**, *78*, 220–230.

(42) Hung, N. G.; Nagy, Z. Kinetics of the Ferrous/Ferric Electrode Reaction in the Absence of Chloride Catalysis. *J. Electrochem. Soc.* **1987**, *134* (9), 2215–2220.

(43) Weber, J.; Samec, Z.; Marecek, V. The Effect of Anion Adsorption on the Kinetics of the Fe3+/Fe2+ Reacion on Pt and Au Electrodes in HClO4. *J. Electroanal. Chem.* **1978**, *89*, 271–288.